Proceedings of the ASME 2012 Conference on Smart Materials, Adaptive Structures and Intelligent Systems SMASIS2012

September 19-21, 2012, Stone Mountain, Georgia, USA

SMASIS2012-7996

DESIGN OF BEND-AND-SWEEP COMPLIANT MECHANISM FOR PASSIVE SHAPE CHANGE

Yashwanth Tummala

Ph.D. Candidate
Dept. of Mechanical and Nuclear Engineering
The Pennsylvania State University
University Park, PA, USA

Aimy Wissa

Ph.D. Candidate
Dept. of Aerospace Engineering
University of Maryland
National Institute of Aerospace
Hampton, VA, USA

Mary Frecker

Professor

Dept. of Mechanical and Nuclear Engineering
The Pennsylvania State University
University Park, PA, USA

James E. Hubbard Jr.

Langley Distinguished Professor Dept. of Aerospace Engineering University of Maryland National Institute of Aerospace Hampton, VA, USA

ABSTRACT

Contact aided compliant mechanisms are a class of compliant mechanisms where parts of the mechanism come into contact with one another during motion. Such mechanisms can have nonlinear stiffness, cause stress-relief, or generate non-smooth paths. New contact aided compliant mechanisms called bend-and-sweep compliant mechanisms are presented in this paper. These bend-and-sweep mechanisms are made up of compliant joints which are alternately located in two orthogonal directions, and they also exhibit nonlinear stiffness in two orthogonal directions. The stiffness properties of these mechanisms, in each direction, can be tailored by varying the geometry of the compliant joints. One application of these mechanisms is in the passive wing morphing of flapping wing UAVs or ornithopters. A design study is conducted to understand the effect of hinge geometry on the deflections and maximum von Mises stress during upstroke and downstroke. It is shown that the bend-and-sweep compliant elements deflect as desired in both the bending and sweep directions.

1. NOMENCLATURE

 R_{in} = Inner radius of a single compliant hinge (m)

 R_{out} = Outer radius of a single compliant hinge (m)

Y-axis = Bending direction

Z-axis = Sweep direction

 g_c = Contact gap between the contact surfaces (m)

 ℓ_{hc} = Length of horizontal cut in fundamental element of second design (m)

 ℓ_{te} = Length of teeth (m)

 ℓ_{vc} = Length of vertical cut in fundamental element of second design (m)

 n_{te} = Number of teeth

 ϕ = Contact angle of the compliant joint (degrees)

 ϕ_{te} = Angle of the teeth (degrees)

2. INTRODUCTION

Contact aided Compliant Mechanisms (CCMs) are a class of compliant mechanisms where the compliant members come into contact with one another to perform a specific task or to improve the performance of the mechanism itself. A wide variety of contact interactions, from a simple case involving single point contact to a more complex case of multiple contacts between different parts of the compliant mechanism

itself, can be used to perform special tasks. These mechanisms were first introduced in the literature by Mankame and Ananthasuresh in 2002 [1]. Such mechanisms can have nonlinear stiffness [2,3], stress relief capabilities [4] and can also generate a non-smooth path [1]. Mankame and Ananthasuresh have presented a displacement delimited contact aided compliant gripper [1]. They have also presented a CCM which uses intermittent contacts to convert reciprocating translation into two output curves to enclose a two dimensional region [5]. Other CCMs that trace prescribed, non-smooth paths in response to a single, monotonically increasing input force were also synthesized by the same authors using topology optimization [6]. Reddy et. al. designed CCMs to trace large, non-smooth paths using topology optimization and finite element analysis (FEA) [7]. Mehta et. al. have designed honeycomb cells with contact elements called Contact Aided Cellular Mechanisms (C³Ms) to obtain stress relief [8]. Cirone et. al. have designed these C³Ms with curved walls for high strain applications [9]. Halverson et. al. have designed a bi-axial CCM for spinal arthroplasty [10]. Cannon and Howell have designed a contact aided compliant revolute joint [11].

The bend-and-sweep compliant mechanism presented in this paper is also a contact aided compliant mechanism. Such a mechanism is designed to have nonlinear stiffness properties in two orthogonal directions. The design of compliant mechanisms with different stiffness properties in orthogonal directions has been considered by some researchers. Bubert et al. have designed a morphing skin using a zero-Poisson honeycomb structure which can achieve 100% in-plane, uniaxial extension but is very stiff in the out-of-plane direction [12]. Vocke III et al. tested this mechanism in a wind tunnel [13]. Barbarino et al. have designed a morphing cellular structure which is flexible in the in-plane direction but is stiff in the out-of-plane direction [14]. This mechanism was designed to achieve chord morphing of helicopter rotor blades.

The bend-and-sweep compliant mechanism presented in this paper is designed to enable passive shape change in an avian-scale ornithopter. Ornithopters, or flapping wing Unmanned Aerial Vehicles (UAVs), have the potential to revolutionize UAV performance in both civil and military sectors [15]. This work aims at improving the performance of these ornithopters during steady level flight by integrating passive compliant mechanisms into the wing structure. Previous work by the authors has shown that such an approach is feasible and that implementation of a 1 Degree Of Freedom (DOF) compliant mechanism resulted in significant improvements in the performance of a test ornithopter [16,17].

To achieve an avian-inspired wing gait in the ornithopter, the outer section of the wing must bend, sweep and twist simultaneously during the upstroke, while remaining fully extended during the downstroke [16]. In this paper, two new contact aided compliant mechanisms called bend-and-sweep compliant mechanisms are presented. Both compliant mechanisms are designed to achieve simultaneous bending

and sweeping of the ornithopter wings. Geometric parameters that determine the stiffness of each of these mechanisms are defined and a design study is conducted to understand their performance.

The remainder of the paper is organized as follows. Section 3 introduces bend-and-sweep compliant mechanism designs, their fundamental elements and their stiffness properties. Section 4 presents the results of finite element analyses to predict the performance of a range of designs. Finally, conclusions and future work are presented in section 5.

3. BEND-AND-SWEEP COMPLIANT MECHANISMS

Bend-and-sweep compliant mechanisms are contact aided compliant mechanisms with tailorable nonlinear stiffness properties. These compliant mechanisms have two orthogonal degrees of freedom, one that will allow in-plane bending and another that will allow out-of-plane bending. Nonlinear stiffness of the mechanism in each direction can be tailored. Two bend-and-sweep compliant mechanisms designs are shown in Figures 1 and 2. Compliant Joints (CJs) are the fundamental elements of both the bend-and-sweep designs. An example design with five compliant joints is pictured in Figure 1. Here, the Y-direction is referred to as the bending direction while Z-direction is referred to as the sweep direction. Hence, the first bend-and-sweep compliant mechanism design, shown in Figure 1, has three compliant joints that result in deformation in the bending direction, while it has two compliant joints that result in deformation in the sweep direction. In this mechanism, the bending and sweep compliant joints are independent of each other.

A second bend-and-sweep compliant mechanism is shown in Figure 2. Unlike in the previous design, the compliant joints of this design are interconnected. As a result when bending occurs in the +Y direction the contact surfaces come into contact, and both the bending and sweep compliant joints lock. On the other hand, when bending occurs in the -Y direction both compliant joints are free to deflect.

The nonlinear stiffness of these designs in either direction was obtained by performing FEA using ANSYS (commercial finite element software). To obtain the bending stiffness of these mechanisms, tip loads were applied in the Y direction. These tip loads were applied at the locations represented by the black square and the yellow triangle shown in Figure 1 and Figure 2. Similarly, to obtain the stiffness in the sweep direction, tip loads were applied in the Z direction. These tip loads were applied at the locations, represented by the black square and the red dot in Figure 1 and Figure 2. The base of the designs, normal to the X-axis, is constrained (as shown in Figure 1 and Figure 2). Solid45, Conta173, and Targe170 finite elements, large deformation quasi-static analysis and multi-linear material properties of DelrinTM (Dupont polymer) were used during the analysis [18,19]. The stiffness plots of these compliant mechanisms are shown in Figure 3. It can be

seen from Figure 3 that both these mechanisms exhibit nonlinear stiffness. It should also be observed from the plot that after contact occurs, the stiffness of the designs increases thus making the stiffness nonlinear.

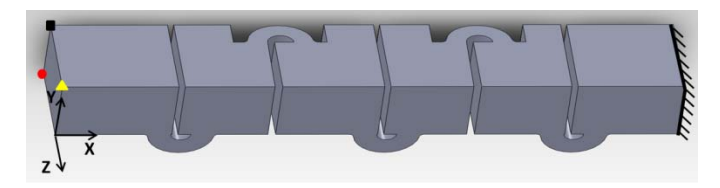


Figure 1 Bend-and-sweep compliant mechanisms, first design. This design has CJs in two orthogonal planes causing two independent DOF motion in the respective orthogonal planes.

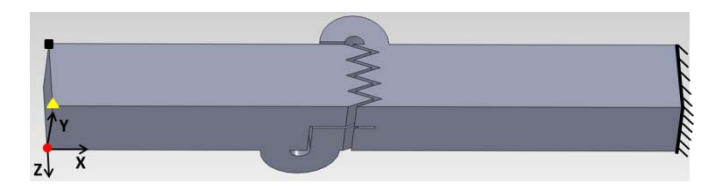


Figure 2 Bend-and-sweep compliant mechanisms, second design. This design also has two CJs in two orthogonal planes but the joints are interconnected causing the sweep CJ to lock whenever the bending CJ is locked.

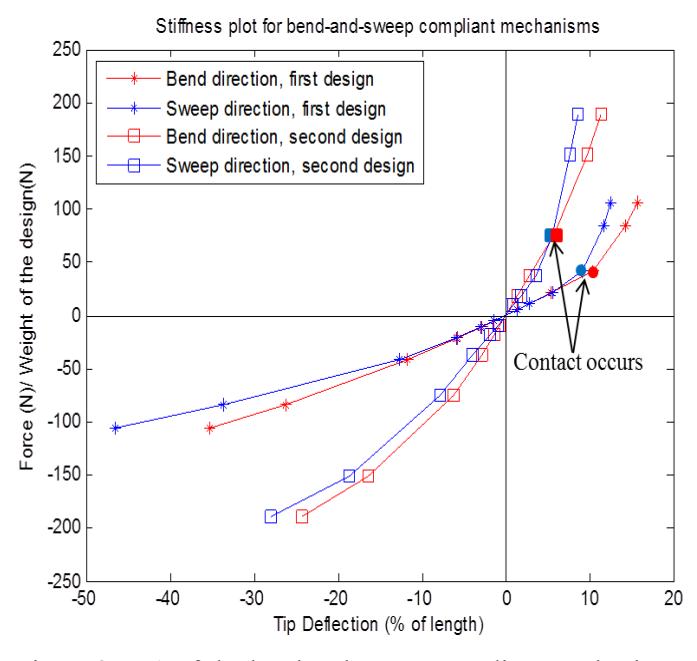


Figure 3 FEA of the bend-and-sweep compliant mechanisms. The stiffnesses are nonlinear and the designs become stiffer when contact occurs.

The stiffness of both compliant mechanisms in the bending and sweep directions can be tailored by changing the geometric parameters of the compliant joints. A fundamental compliant element that constitutes the first design is shown in Figure 4. Such an element has one bending CJ and one sweep CJ. The geometric parameters of a CJ that affect its stiffness are the contact gap (g_c) , contact angle (ϕ) , inner radius (R_{in}) and outer radius (R_{out}) of the compliant hinge (shown in Figure 4).

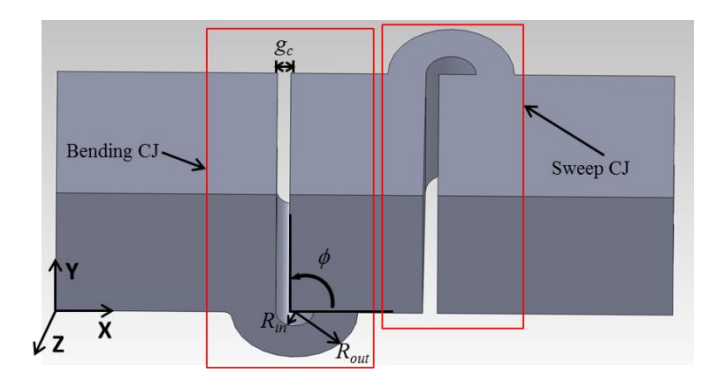


Figure 4 Fundamental compliant element of the first design. The geometric variables shown affect the stiffness in both bending and sweep directions.

A fundamental compliant element of second design is shown in Figure 5. The geometric parameters that affect the stiffness of the second design are inner and outer radii of bending CJ and sweep CJ, length of horizontal cut (ℓ_{hc}), length of vertical cut (ℓ_{hc}), contact gap (g_c), number of teeth (n_{te}), angle of the teeth (ϕ_{te}), and length of teeth (ℓ_{he}), as shown in Figure 5. The contact gap for this element is defined as the gap between any two contact surfaces. There are four teeth that make up the contact surfaces of the sweep compliant joint in the fundamental element shown ($n_{te} = 4$). These teeth are also part of the bending compliant joint, hence causing the sweep CJ to lock when the bending CJ locks.

Both fundamental compliant elements are analyzed for a range of values of the geometric variables as part of a design study. Results of the design study and the potential application to passive shape change in an avian-scale ornithopter are presented in the next section.

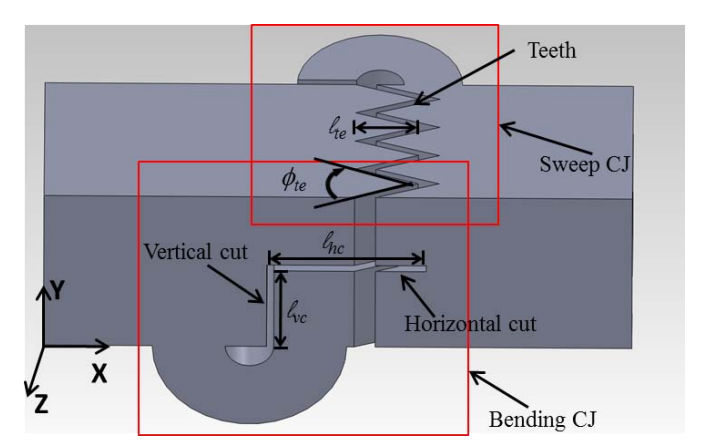


Figure 5 Fundamental element of second design. The geometric variables shown affect the stiffness in both bending and sweep directions.

4. DESIGN STUDY

The bend-and-sweep compliant mechanisms are passive, and are designed to deform as a natural consequence of the aerodynamic loads acting on the ornithopter during flight. Hence they are designed to provide the desired bend-andsweep of the wings as a result of the lift and drag forces experienced by the ornithopter during straight and level flight. Bending of the wings is achieved because of the lift forces while sweep is mainly due to the drag forces. Unlike the lift forces which change their direction during a single flapping cycle, the drag forces always act in one direction. As a result, the bend-and-sweep compliant mechanism should cause the wings to sweep during the upstroke but will have to be stiff in the sweep direction during downstroke even though the direction of the drag forces remains the same. To accurately predict the deflections of the bend-and-sweep compliant mechanisms during the upstroke and downstroke, an estimate of the aerodynamic loads acting on the wing structure is needed.

To determine the aerodynamic loads acting on the ornithopter wing structure, strain gage experiments were conducted by the authors and presented in [16]. Based on these results it was determined that the maximum magnitude of the integrated lift loads during a flapping cycle at 5 Hz was 10N [3]. During bench top testing of the ornithopter, it was found that the ornithopter generates a peak thrust of 0.7lbf at a flapping frequency of 5 Hz and zero forward velocity [16]. This suggests that each wing generates a thrust of 0.35lbf (1.56N). The ornithopter is airborne and capable of forward flight at a flapping frequency of 5Hz. This implies that the thrust forces produced by the ornithopter at this frequency can overcome the drag forces. Hence we assume that the maximum drag force that the test ornithopter's wing may experience is 1.56N which is equal to the thrust force produced by one ornithopter wing at a flapping frequency of 5Hz.

Two sets of loads were applied to simulate the upstroke and downstroke conditions in this design study. During the upstroke, lift loads are present in the -Y direction, as well as drag loads in the -Z direction (shown in Figure 6). During the downstroke, the lift loads are present in the +Y direction, as well as the drag forces in the -Z direction (Figure 7). These loads are approximated using concentrated loads applied at the free end of the compliant mechanisms. A tip load of 10N was applied in the bending direction to simulate the integrated lift forces. A tip load of 1.56N was applied in the sweep direction (Figure 6 and Figure 7) to simulate drag forces.

The fundamental compliant elements, each with one bending CJ and one sweep CJ were considered. To understand the effect of geometric parameters on the stiffness of the bendand-sweep compliant mechanisms, sixteen different variations of the designs for each type were generated by varying the inner and outer radii of the CJs. Rout for bending CJ was increased from 6mm to 7mm in steps of 0.25mm. R_{in} for bending CJ was increased from 3.5mm to 4.5mm in steps of 0.25mm. R_{out} for sweep CJ was increased from 6.75mm to 7.25mm in steps of 0.25mm while R_{in} for sweep CJ was increased from 4.75mm to 5.75mm in steps of 0.25mm. Same range of radii was used for both first and second designs. Also, similar loading conditions were used for all the first and second designs. Based on the size of the test ornithopter, all the designs were constrained to fit within an imaginary box with dimensions 1.5" x 0.75" x 0.75" (38.1mm x 19.05mm x 19.05mm). These designs were first generated in Solidworks and then imported to ANSYS for FEA. Solid45, Conta173, Targe170 finite elements, large displacement quasi-static analysis, and multi-linear material properties of DelrinTM were used during the analysis [18,19]. Contact elements were used for the downstroke simulations. Although the application is dynamic in nature, quasi-static analysis was used because contact can be modeled efficiently using quasi-static analysis.

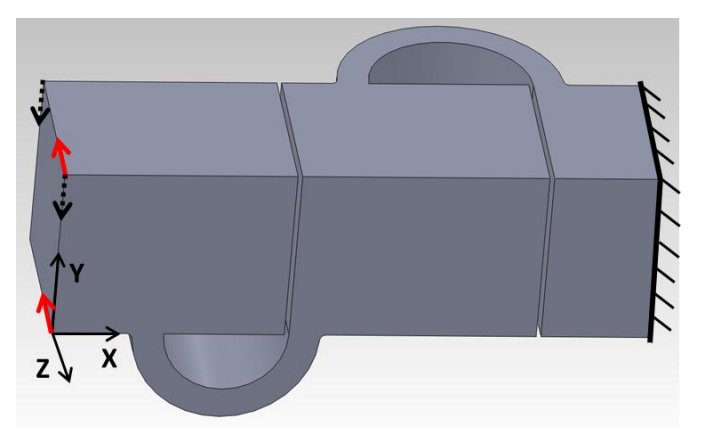


Figure 6 Applied loads and boundary conditions on the first design during the upstroke. Red arrows indicate drag forces, dashed arrows indicate lift forces.

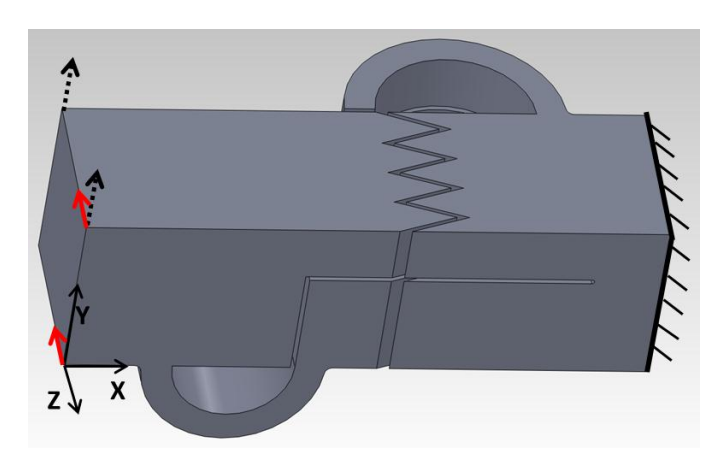


Figure 7 Applied loads and boundary conditions on the second design during the downstroke. Red arrows indicate drag forces, dashed arrows indicate lift forces.

The metrics that were used for comparison in the design study are the maximum von Mises stress observed in the designs, and the tip displacement of the designs in the Y (bending) and Z (sweep) directions. The three metrics are presented as three 2-D plots in Figures 8 through 10. Each variation in the CJ radii represents a new design. Each design is represented by two points in Figures 8 through 10: a blue point and a red point for the upstroke and downstroke performance, respectively.

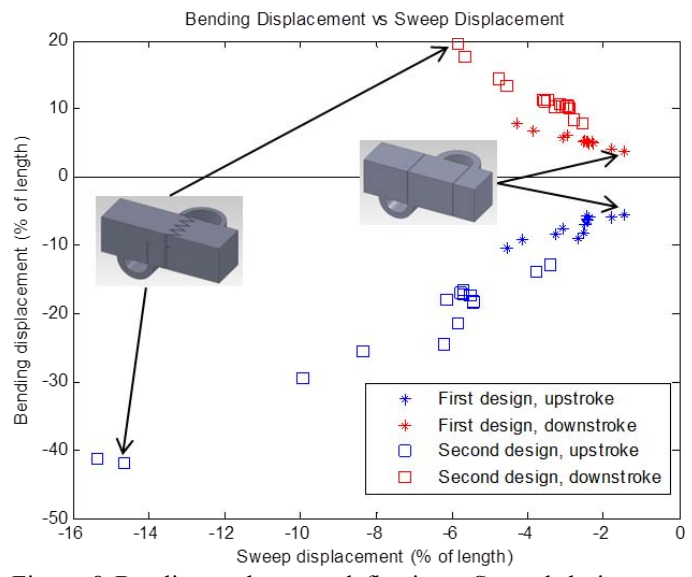


Figure 8 Bending and sweep deflections. Second designs are less stiff than first designs, and have lower sweep displacement during downstroke than upstroke.

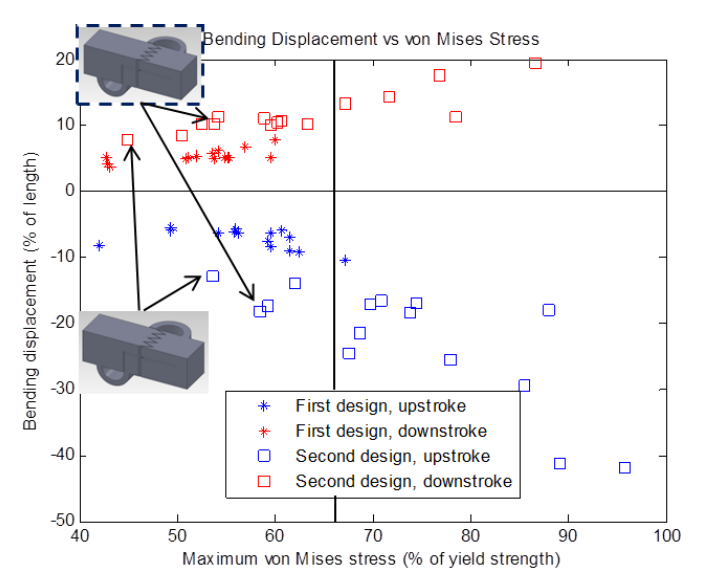


Figure 9 Bending displacement and maximum von Mises stress. Almost all the first designs are acceptable while only four of the second designs are acceptable.

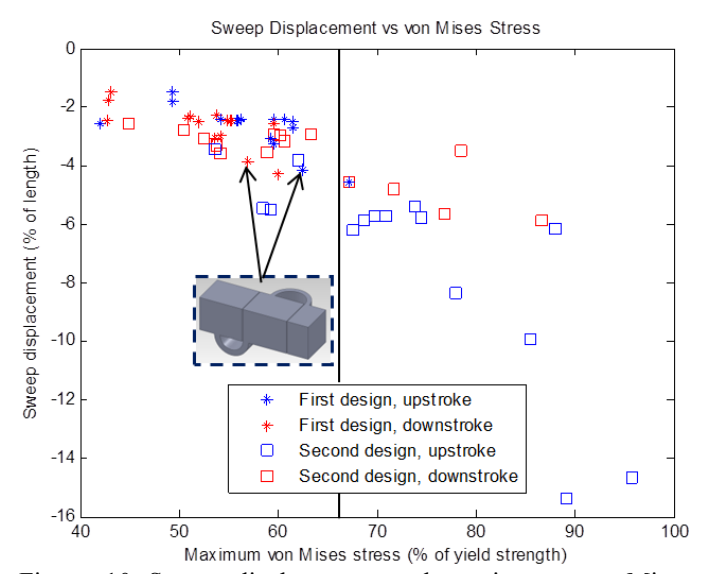


Figure 10 Sweep displacement and maximum von Mises stress. Sweep displacement is always negative because the drag forces do not change direction during a flapping cycle.

In order for the compliant mechanisms to be useful in the avian-scale ornithopter application, the design process aimed to maximize bending and sweep displacements during upstroke while minimizing the bending and sweep displacements during downstroke. Also, minimum von Mises stress is desired in all the designs during both upstroke and downstroke.

Figure 8 compares the bending and sweep displacement of all the designs, both first and second, during upstroke and downstroke. During upstroke, the bending deflection is in the –Y direction and the sweep deflection is in the –Z direction.

During downstroke, the bending deflection is in the +Y direction and the sweep deflection is in the -Z direction. The sweep deflection is still negative during downstroke because the direction of the drag force was not changed. Deflections during downstroke are desired to be as small as possible in either direction. It can be seen from Figure 8 that the first designs are stiffer than the second designs because both the blue and red stars are closer to the origin. Also, the sweep displacement of the first designs is about the same during both upstroke and downstroke which is undesired. On the other hand, all of the second designs are less stiff with more deflection during upstroke and downstroke. Their stiffness could be increased by changing the radii of the CJs. But an important observation that can be made from the second designs is that their sweep displacement is lower during downstroke than during upstroke (about 50% lower), which is desired and expected as well because of the interconnection between the CJs. Ideally, all the designs would have downstroke deflections very close to the origin.

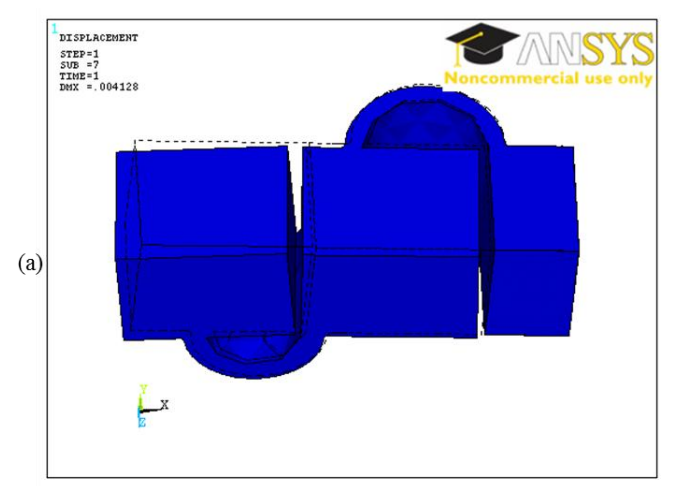
Figure 9 compares the bending displacement and maximum von Mises stress observed in the designs. The material chosen for the designs was Delrin which has a yield stress of 45MPa. If a safety factor of 1.5 is chosen for the designs, then all the acceptable designs are located to the left of the vertical line drawn at 66.67%. Two sample acceptable designs are shown in the plot. It can be observed that almost all the first designs are acceptable in terms of stress while only four of the second designs are acceptable. Although both the first and second designs have similar inner and outer radii of the CJs, their deflections are very different because of the different contact surfaces. It should also be noted that many of the second designs have large von Mises stresses. They also have higher bending deflections during downstroke when compared to their first design counterparts.

Figure 10 compares sweep displacement and maximum von Mises stress observed in all the designs during upstroke and downstroke. Feasible designs in this plot again are located to the left of the vertical line drawn at 66.67%. All the first designs in this plot have lower von Mises stresses and lower sweep deflections than the corresponding second designs. While on the other hand, the second designs have higher sweep deflections and higher von Mises stresses. As was pointed out in Figure 8, the sweep deflection is always negative for both upstroke and downstroke. Ideally designs with high sweep deflection during upstroke, low sweep deflection during downstroke and low von Mises stresses are desired.

The deformed shapes of a typical first design during upstroke and downstroke are shown in Figure 11(a) and Figure 12(a), respectively. Von Mises stress contour plots of the same design during upstroke and downstroke are shown in Figure 11(b) and Figure 12(b), respectively. This design is also indicated in Figure 10 by a black, dashed outline.

Figure 11 suggests that the compliant mechanism bends and sweeps. It can also be seen from the figure that the sweep

CJ experiences large von Mises stress during the deformation. Figure 12 shows that during downstroke, the contact surfaces of the sweep CJ do not come into contact because the drag forces do not change their direction. On the other hand, bending CJ is locked because of the lift forces. It should be noted from both these figures that the deformation of this design is, qualitatively, as expected and sweep CJ experiences higher von Mises stress than the rest of the design during both upstroke and downstroke.



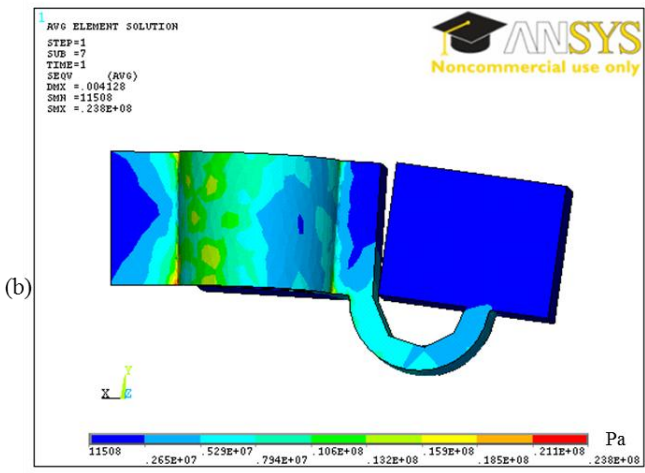
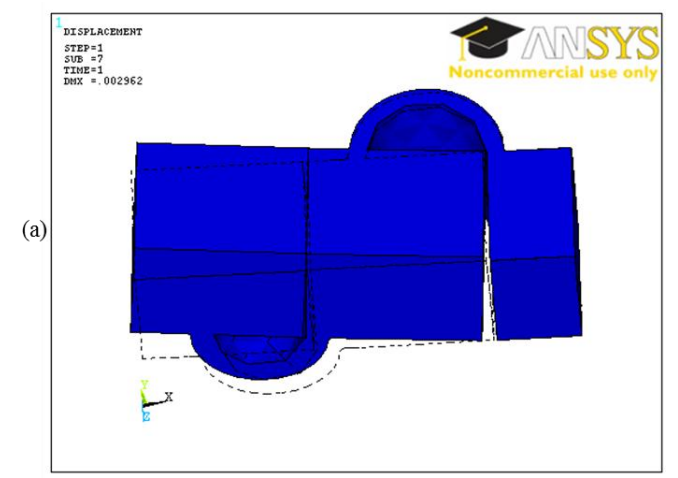


Figure 11 (a) Deformed shape of a typical first design during upstroke. The undeformed shape is indicated by the dashed lines. (b) Back view of the von Mises stress contour plot for the same design during upstroke. The von Mises stress is highest during sweep.



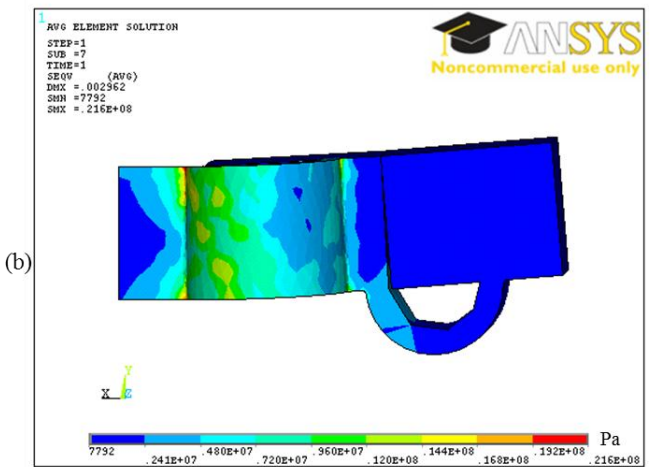
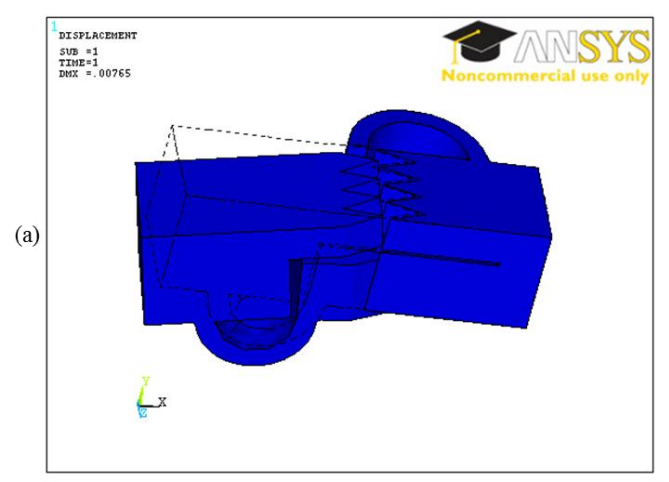


Figure 12 (a) Deformed shape of a typical first design during downstroke. The undeformed shape is indicated by the dashed lines. (b) Back view of the von Mises stress contour plot for the same design during downstroke. Some sweep deformation is observed during downstroke.

The deformed shapes of a typical second design during upstroke and downstroke with its undeformed edge are shown in Figure 13(a) and Figure 14(a), respectively. Von Mises stress contour plots of the same design during upstroke and downstroke are shown in Figure 13(b) and Figure 14(b), respectively. This design is also indicated in Figure 9 by a black, dashed outline.

Figure 13(a) and Figure 14(a) suggest that the design deforms as expected; i.e., the design bends and sweeps as desired during upstroke while both the CJs lock during downstroke. Figure 13(b) and Figure 14(b) show the back view of the von Mises stress contour plots. It can be seen that the maximum stress is located at the base of the sweep CJ. From the above four figures (Figures 11 through 14) it can be observed that the first designs are stiff when compared to second designs.



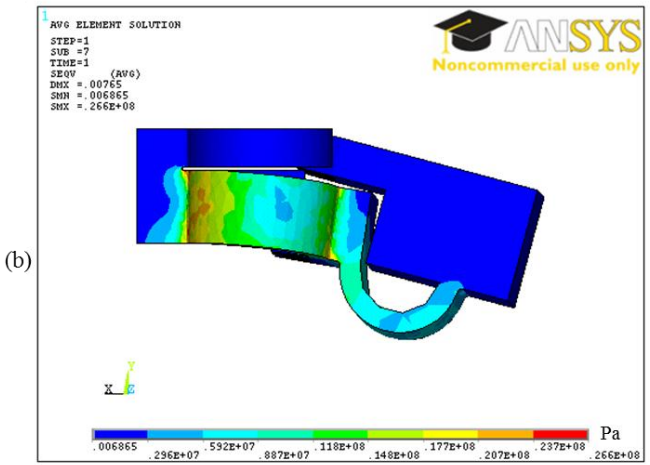
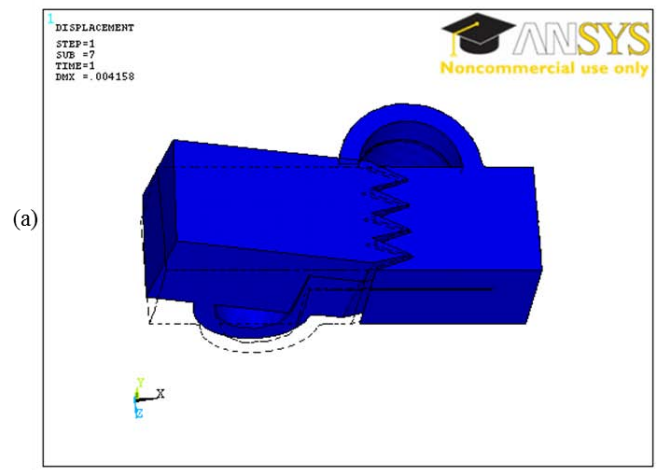


Figure 13 (a) Deformed shape of a typical second design during upstroke. The undeformed shape is indicated by the dashed lines. (b) Back view of the von Mises stress contour plot for the same design during upstroke. The von Mises stress is highest during sweep.



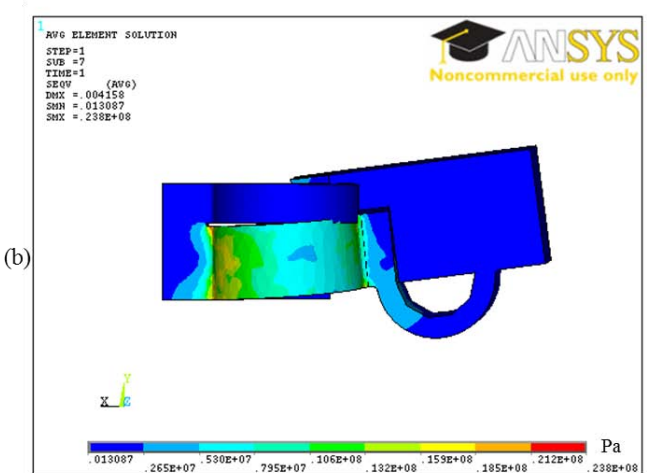


Figure 14 (a) Deformed shape of a typical second design during downstroke. The undeformed shape is indicated by the dashed lines. (b) Back view of the von Mises stress contour plot for the same design during downstroke. Both the sweep and bending CJs are locked during downstroke.

5. CONCLUSIONS & FUTURE WORK

Two bend-and-sweep compliant mechanisms with tailorable nonlinear stiffness in two orthogonal directions were developed for passive shape change. Geometric parameters that define the stiffness of each of the mechanisms were presented. Nonlinear finite element analysis was used to analyze the fundamental elements of these mechanisms and the results suggested that the first and second designs deform as expected during upstroke and downstroke. The sweep CJs in both the designs experience the largest von Mises stress during both upstroke and downstroke. The results of the design study also suggested that second designs could be appropriate for the ornithopter application because they experience the lowest sweep deflection during downstroke. They also have high bending deflection during upstroke as

desired. The stress distribution can be improved and the bending deflections during downstroke could be minimized through a formal design optimization procedure, which is part of the future work.

6. ACKNOWLEDGEMENTS

The authors gratefully acknowledge the support of AFOSR grant number FA9550-09-1-0632. The computational work was supported in part through instrumentation funded by the National Science Foundation through grant OCI–0821527. The resources of the NASA Langley Research Center, Pennsylvania State University, the University of Maryland and the Morpheus Lab are also appreciated.

7. REFERENCES

- [1] Mankame, N. D. and Ananthasuresh, G. K., 2002, "Contact aided compliant mechanisms: Concept and preliminaries", *International Design Engineering Technical Conferences and Computers and Information in Engineering Conference*, Montreal, QC, Canada, Web Portal ASME 109-121.
- [2] Tummala, Y., Wissa, A., Frecker, M., Hubbard Jr., J. E., 2010, "Design of a Passively Morphing Ornithopter Wing Using a Novel Compliant Spine", Proceedings of Smart Materials, Adaptive Structures and Intelligent Systems Conference, Philadelphia, PA, United States.
- [3] Tummala, Y., Wissa, A., Frecker, M., Hubbard Jr., J. E., 2011, "Design Optimization of a Compliant Spine for Dynamic Applications", *Proceedings of Smart Materials, Adaptive Structures and Intelligent Systems Conference*, Scottsdale, AZ, United States.
- [4] Mehta, V., Frecker, M. and Lesieutre, G., 2008, "Contact-aided compliant mechanisms for morphing aircraft skin", *Modeling, Signal Processing, and Control for Smart Structures 2008*, USA, SPIE - The International Society for Optical Engineering.
- [5] Mankame, N. D. and Ananthasuresh, G. K., 2004, "A novel compliant mechanism for converting reciprocating translation into enclosing curved paths," *Journal of Mechanical Design*, 126(4), 667-72.
- [6] Mankame, N. D. and Ananthasuresh, G. K., 2007, "Synthesis of contact-aided compliant mechanisms for non-smooth path generation," *International Journal for Numerical Methods in Engineering*, 69, 2564-2605.
- [7] Reddy, B. V. S. N., Naik, S. V. and Saxena, A., 2012, "Systematic Synthesis of Large Displacement Contact-Aided Monolithic Compliant Mechanisms," *Journal of Mechanical Design*, 134(1), 011007-12.

- [8] Mehta, V., Frecker, M. and Lesieutre, G. A., 2009, "Stress relief in contact-aided compliant cellular mechanisms," *Journal of Mechanical Design*, 131, 0910091-09100911.
- [9] Cirone, S. A., Hayes, G. R., Babcox, B. L., Frecker, M., Adair, J. H. and Lesieutre, G. A., 2011, "Design, fabrication and testing of contact-aided compliant cellular mechanisms with curved walls", *Active and Passive Smart Structures and Integrated Systems* 2011, USA, SPIE The Society for Optical Engineering
- [10] Halverson, P. A., Howell, L. L. and Bowden, A. E., 2008, "A flexure-based bi-axial contact-aided compliant mechanism for spinal arthroplasty", International Design Engineering Technical Conferences & Computers and Information in Engineering Conference, Brooklyn, New York.
- [11] Cannon, J. R. and Howell, L. L., 2005, "A compliant contact-aided revolute joint," *Mechanism and Machine Theory*, 40(11), 1273-1293.
- [12] Bubert, E. A., Woods, B. K. S., Keejoo, L., Kothera, C. S. and Wereley, N. M., 2010, "Design and Fabrication of a Passive 1D Morphing Aircraft Skin," *Journal of Intelligent Material Systems and Structures*, 21(17), 1699-717.
- [13] Vocke III, R. D., Kothera, C. S., Woods, B. K. S. and Wereley, N. M., 2011, "Development and testing of a span-extending morphing wing," *Journal of Intelligent Material Systems and Structures*, 22(9), 879-890.
- [14] Barbarino, S., Gandhi, F. and Webster, S. D., 2011, "Design of extendable chord sections for morphing

- helicopter rotor blades," *Journal of Intelligent Material Systems and Structures*, 22(9), 891-905.
- [15] Shyy, W., Berg, M. and Ljungqvist, D., 1999, "Flapping and Flexible Wings for Biological and Micro Air Vehicles," *Progress in Aerospace Sciences*, 35(5), 455-505.
- [16] Wissa, A., Tummala, Y., Hubbard Jr., J. E., Frecker, M., 2011, "Testing of Novel Compliant Spines for Passive Wing Morphing", Proceedings of Smart Materials, Adaptive Structures and Intelligent Systems Conference, Scottsdale, AZ, United States.
- [17] Wissa, A., Tummala, Y., Hubbard Jr., J. E., and Frecker, M., 2012, "Passively Morphing Ornithopter Wings using a Novel Compliant Spine: Design and Testing," *Smart Materials and Structures (accepted April 2012)*.
- [18] Dupont, 2011, "http://plastics.dupont.com/plastics/pdflit/americas/delrin/230323c.pdf".
- [19] Olympio, K. R., 2006, "Design of A Passive Flexible Skin for Morphing Aircraft Structures", M.S. thesis, The Pennsylvania State University.